

Galactic archæology of a thick disc: excavating ESO 533-4 with VIMOS [★]

S. Comerón^{1,2}, H. Salo¹, J. Janz³, E. Laurikainen^{1,2}, and P. Yoachim⁴

¹ University of Oulu, Astronomy and Space Physics, P.O. Box 3000, FI-90014, Finland
e-mail: seb.comeron@gmail.com

² Finnish Centre of Astronomy with ESO (FINCA), University of Turku, Väisäläntie 20, FI-21500, Piikkiö, Finland

³ Centre for Astrophysics and Supercomputing, Swinburne University, Hawthorn, VIC 3122, Australia

⁴ Department of Astronomy, University of Washington, Box 351580, Seattle, WA 98195, USA

Preprint online version: February 15, 2019

ABSTRACT

The disc of galaxies is made of the superposition of a thin and a thick disc. Star formation is hosted in the thin discs and contributes to their growth. Thick discs are made of old stars. The formation mechanisms of thick discs are under discussion. Thick discs might have formed either at high redshift on a short time-scale or might have been built slowly over a Hubble-Lemaître time. They may have an internal or an external origin. Here we adopt a galactic archæology approach to study the thick disc of ESO 533-4, i.e., we study in detail the kinematics and the stellar populations of this galaxy. ESO 533-4 is a Southern, nearby, and almost bulgeless galaxy. We present the first ever Integral Field Unit spectroscopy of an edge-on galaxy with enough depth and quality to study the thick disc. We exposed ESO 533-4 with the blue grism of the VIMOS instrument of the VLT for 6.5 hours. The field of view covered an axial extent from $\sim 0.1 r_{25}$ to $\sim 0.7 r_{25}$ where r_{25} is the 25 mag arcsec⁻² isophotal radius. This corresponds to the range from ~ 1 kpc to ~ 7 kpc. We used pPXF and the MILES library to obtain velocity and stellar population maps. We compared our kinematic data with simple GADGET-2 models.

The apparent rotational lag of the thick disc of ESO 533-4 is compatible with that expected from the combinations of two effects: differential asymmetric drift and the projection effects arising from studying a disc a few degrees ($2 - 3^\circ$) away from edge-on. Thus, ESO 533-4 contains little or no counterrotating material. This is compatible with three formation scenarios: the secular dynamical heating of an initially thin disc, the formation of the thick disc at high redshift in an early turbulent disc phase, and the creation of a thick disc in a major merger event. If happening in all galaxies, this last mechanism would cause retrograde thick discs in half of them. Such retrograde discs have not been observed in the five massive disc galaxies (circular velocity $v_c \gtrsim 120$ km s⁻¹) for which the kinematics of the thick disc is known. The stellar populations map indicates that the populations of the thin and the thick discs are possibly separated in the Age – $\log(Z/Z_\odot)$ plane. This would imply that the thin and the thick discs are made of two distinct stellar populations. Although the stellar population results are not conclusive due to the high dust extinction in ESO 533-4, they do not favour a secular evolution origin for the thick disc. Hence, we suggest that the thick disc of ESO 533-4 formed in a relatively short event.

Key words. galaxies: individual (ESO 533-4) – galaxies: kinematics and dynamics – galaxies: spiral – galaxies: structure – galaxies: evolution – galaxies: formation

1. Introduction

1.1. Thick discs and galactic archæology

We know with absolute certainty that our universe contains galaxies (Curtis 1917; Öpik 1922; Hubble 1925). Another fact established with almost the same degree of certitude is that the initial state of the universe was a hot Big Bang (Lemaître 1931; Gamow 1946; Alpher & Herman 1949; Penzias & Wilson 1965). It follows that the products of the primordial nucleosynthesis somehow assembled and evolved into the galaxies that we observe roughly a Hubble-Lemaître time after creation. The current cosmological paradigm is Λ CDM (Ade et al. 2015, for its more recent parameter determination), where the energy budget of the universe is dominated by elusive dark matter and a positive cosmological constant. Within that paradigm, the evolution of galaxies is driven by a combination of interactions with the environment (nurture, e.g., Toomre 1977) and internal evolution

(nature, e.g., Kormendy & Kennicutt 2004; Athanassoula 2013). However, the details and the specific weight of each of these two families of processes in the galaxy construction and subsequent evolution still elude us.

One of the most mysterious remnants of galaxy formation and evolution are thick discs. Seen as roughly exponential vertical excesses of light in edge-on galaxies a few thin disc scale-heights above the galaxy mid-planes, their origin is still a matter of debate more than three decennia after their discovery (Burstein 1979; Tsikoudi 1979). Nowadays, all disc galaxies where thick discs have been searched for have been found to host one or even two of them (Yoachim & Dalcanton 2006; Comerón et al. 2011c,b). The following scenarios have been proposed to explain their formation:

- **External fast processes:** the thick disc is the consequence of the merger of two or more gas-rich galaxies during the initial assembly process (Brook et al. 2004).
- **Internal fast processes:** the thick disc is born thick due to the turbulent and clumpy nature of the first

[★] Based on observations made at the European Southern Observatory using the Very Large Telescope under programme 091.B-0228(A).

Table 1. Summary of the signatures predicted in the thick disc formation scenarii

Scenario	External/ Internal	Fast/ Secular	Counterrotating material in the thick disc	Chemical and/or age discontinuity between the thin and thick discs
Merger of gas-rich galaxies	External	Fast	Possibly ^a	Yes
Turbulent early disc	Internal	Fast	No ^b	Yes
Accretion of stars from satellites	External	Secular	Possibly ^a	Yes
Heating by satellites	External	Secular	No	No
Internal heating	Internal	Secular	No	No

^(a) Those processes would cause some amount of counterrotating material provided that some of the mergers are retrograde. ^(b) In the Bournaud et al. (2014) simulations, some counterrotating stars are created in this process. The fraction of retrograde stars decreases as a function of the mass of the galaxy. A high- z galaxy with a $1.4 \times 10^{10} M_{\odot}$ baryonic mass, similar to the mass of ESO 533-4's thick disc, would have 2.2% of counterrotating stars (F. Bournaud, private communication). Such a small fraction of counterrotating stars would be undetectable with the techniques used in this paper.

discs (Elmegreen & Elmegreen 2006; Bournaud et al. 2009; Comerón et al. 2014).

- **External secular processes:** the thick disc is made of stars stripped from infalling satellites (Abadi et al. 2003) and/or by the disc dynamical heating caused by them (Quinn et al. 1993; Qu et al. 2011). We call these processes secular because minor mergers are much slower than major mergers due to the weaker dynamical friction. Also, according to Λ CDM, several of these events can occur in a Hubble-Lemaître time (e.g., several tens of minor mergers causing tidal features are expected in Johnston et al. 2008).
- **Internal secular processes:** the thick disc is caused by dynamical heating due to disc overdensities (Villumsen 1985) and/or the radial migration of stars (Schönrich & Binney 2009; Loebman et al. 2011). Radial migration as a viable mechanism to build thick discs is contested by Minchev et al. (2012) and Vera-Ciro et al. (2014).

It is likely that a combination of two or more of these scenarii contributed to the thick disc formation. Actually, some mechanisms such as secular internal heating must always occur to some extent. In Comerón et al. (2012) we suggested that thick discs in low and high-mass galaxies might have different dominant formation mechanisms. This is because there is a clear bimodality in the ratio of thick to thin disc masses as a function of the total galaxy mass: high-mass galaxies have the same ratio irrespectively of the galaxy total mass whereas for low-mass galaxies the ratio decreases as the total galaxy mass increases. The fact that most high-mass galaxies have a roughly similar thin/thick disc mass ratio (Comerón et al. 2014) suggests the possibility that the same combination of mechanisms has built them. The dividing line between low- and high-mass galaxies is found at a circular velocity $v_c \approx 120 \text{ km s}^{-1}$ (suggested by Yoachim & Dalcanton 2006, 2008b) which corresponds to a baryonic mass of $M \sim 10^{10} M_{\odot}$ when using the Tully-Fisher relation in Zaritsky et al. (2014).

A particular model (Minchev et al. 2015) which proposes a thick disc created through a combination of internal and external secular heating mechanisms is relevant in later sections of the Paper. In this model, each of the mono-age populations of a galaxy is distributed in a flared disc. The younger stellar populations have a longer scale-length than the older ones. The superposition of a series of flares at different radii produce what in photometric decompositions has been identified as the thick disc. The result of this model is a galaxy with no apparent flare even if the individual mono-age populations do flare.

Due to cosmological dimming and resolution problems, it is often impractical to tackle galaxy evolution issues by observing highly redshifted objects. An alternative is the so-called galactic

archaeology, which consists in studying the structures of redshift $z \sim 0$ galaxies with great detail to infer their origin. Thick discs are ideal targets for galactic archaeology because different formation scenarii predict distinct kinematical and chemical signatures as summarized in Table 1.

So far, attempts to do galactic archaeology in external edge-on galaxies to study thick discs have been mostly based in photometric decompositions (Yoachim & Dalcanton 2006; Comerón et al. 2011a, 2012). The exception is the work by Yoachim & Dalcanton (2008b,a) where single-slit spectroscopy was used to study the thin and the thick discs. They found that the thick discs are made of old stars and that the thick discs of some low-mass galaxies contain counterrotating stars. None of the three massive galaxies in their sample had measurable amounts of retrograde stars. The problem that arises from single-slit observations is that one has to rely on photometric thin/thick decompositions to find the range of heights where the thick disc dominates before placing the slit. Ideally, we would like to be able to observe galaxies in a wide range of heights, so no assumptions on the extent of the thick disc have to be made a priori.

1.2. ESO 533-4

In this Paper we present the first integral field spectroscopy study of the thin/thick structure of an edge-on disc. We used the Visible Multi-Object Spectrograph of the Very Large Telescope (VIMOS; Le Fèvre et al. 2003). The selected target was ESO 533-4. This galaxy has been part of the sample of our recent thick disc studies (Comerón et al. 2012, 2014). The target was chosen because of:

- Its small central mass concentration (CMC), and hence, presumably little effect of a central spheroid on the thin and thick disc kinematics.
- Its relatively small angular size, so a large fraction of the disc could be covered by the VIMOS field of view (FOV).
- A brighter than average thick disc that starts to dominate at $m_{3.6\mu\text{m}}(\text{AB}) \approx 22 \text{ mag arcsec}^{-2}$ (Comerón et al. 2012), so that thick disc spectra can be obtained with a few hour exposure.

A summary of the properties of ESO 533-4 is presented in Table 2. There is a disagreement on the stage of the galaxy in the literature. Its small CMC makes it look late-type (Sc; de Vaucouleurs et al. 1991), but its smooth aspect in $3.6\mu\text{m}$ has recently caused it to be classified as an $S0_c^0$ (Buta et al. 2015). ESO 533-4 has a baryonic mass $M \sim 3 \times 10^{10} M_{\odot}$, so it is a high-mass galaxy. A $3.6\mu\text{m}$ image from the Spitzer Survey

Table 2. Parameters of ESO 533-4

Parameter	Value	Source
RA (J2000.0)	22 ^h 14 ^m 03.02	1
Dec (J2000.0)	−26°56′15″.8	1
$M_{3.6\mu\text{m}}(\text{AB})$	−20.52	2
Type	Sc? sp	3
	S0 _c ^o sp/E(d)8	4
v_{sys} (helio-centric)	$2596 \pm 3 \text{ km s}^{-1}$	5
D	39.8 Mpc	6
1″ physical size	193 pc	6
v_c	$147.5 \pm 2.2 \text{ km s}^{-1}$	7
r_{25}	54″.6	7
Luminosity profile	Type 2 break	8
M_g	$(680 \pm 20) \times 10^7 M_{\odot}$	9
M_{CMC}	$(19 \pm 2) \times 10^7 M_{\odot}$	9
M_t	$(1500 \pm 300) \times 10^7 M_{\odot}$	10
M_T	$(1100 \pm 200) \times 10^7 M_{\odot}$	10

References. (1) Skrutskie et al. (2006); (2) Muñoz-Mateos et al. (2015); (3) de Vaucouleurs et al. (1991); (4) Buta et al. (2015); (5) NED; (6) from NED average of redshift-independent distances; (7) HyperLeda (Makarov et al. 2014); (8) Comerón et al. (2012); (9) atomic gas disc mass (M_g) and CMC mass (M_{CMC}) from Comerón et al. (2014); (10) thin disc mass (M_t) and thick disc mass (M_T) from this Paper.

of Stellar Structure in Galaxies (S⁴G; Sheth et al. 2010) is presented in Figure 1.

2. The thin/thick disc decomposition of ESO 533-4

In Comerón et al. (2012), we made thin/thick disc decompositions of ESO 533-4 for the symmetrized $3.6\mu\text{m} + 4.5\mu\text{m}$ luminosity profiles in four bins perpendicular to the galaxy mid-plane. The discs were assumed to be in hydrostatic equilibrium following the formalism by Narayan & Jog (2002). We accounted for the gravitational effect of a thin gas disc with 20% of the surface mass density of the thin disc. Several simplifying assumptions were made such as similar scale-lengths for the thin and the thick discs, the disc not to be too submaximal in its inner parts, vertical isothermality, and roughly constant scale-heights with changing radii.

In Comerón et al. (2012) we convolved our solutions with a Gaussian kernel to account for the Point Spread Function (PSF) of the S⁴G images. The kernel had a 2″.2 full width at half maximum (FWHM). However, the S⁴G PSF is now known to have faint but extended wings not accounted for by a Gaussian. Here we redo the fits by using the S⁴G symmetrized PSF (Salo et al. 2015). Here we produce our fit using only the $3.6\mu\text{m}$ band, because that is the one for which we have the detailed PSF model.

In this Paper, we use the sky values from the S⁴G Pipeline 3 (Muñoz-Mateos et al. 2015) instead of our own sky determinations. To do the fit, we use IDL’s CURVEFIT instead of our own minimization routine (described in Comerón et al. 2011a). As in Comerón et al. (2012), we use a ratio of mass-to-light ratios of the thick and thin discs $\Upsilon_T/\Upsilon_t = 1.2$. The $\Upsilon_T/\Upsilon_t = 1.2$ value comes from studying the spectral energy distributions resulting from the Milky Way star formation history models by Nyktyuk & Mishenina (2006) for the thin and the thick discs (Comerón et al. 2011a). The maximum height of the fit was selected as that beyond which it is not possible to make a two disc component fit (the mean squared difference between the observed profile and the fit becomes larger than $0.01 (\text{mag arcsec}^{-2})^2$ at that height). What limits the height of the



Fig. 1. $3.6\mu\text{m}$ image of ESO 533-4 from the S⁴G. The red cross indicates the centre of the galaxy and the region with a green border is that studied in this Paper. North is up and East is left. The white solid lines perpendicular to the galaxy mid-plane show the four axial bins used for the luminosity profile fits in Figure 2. The dash-dot lines indicate the heights over which the profiles were fit. The solid lines parallel to the galaxy mid-plane correspond to the height above which 90% of the light comes from the thick disc. The numbers are used to associate the bins to the fits in Figure 2.

fitting region is the presence of scattered light of point-sources in the field and background gradient issues. The extent of the fitting range covers over four thick disc scale-heights.

The new thin/thick disc fits are very similar to those in Comerón et al. (2012), which indicates that the errors introduced by approximating the PSF with a Gaussian function were small. The symmetrized PSF used here covers 15″ in radius. The thick disc dominates the luminosity profiles down to $z \approx 5''$ ($\sim 1 \text{ kpc}$), which is a height safely smaller than the radius of the modelled PSF. If we consider our fitted thin disc, we find that the extra light added to $|z| > 5''$ is about 4% of the observed emission. Therefore, we can discard the possibility that the thick disc is an artefact caused by scattered light as suggested by Sandin (2015).

The new fits indicate a slightly higher ratio of surface densities between the thick and the thin disc (Σ_T/Σ_t) compared to Comerón et al. (2012), which slightly increases the mass ratio of the two discs: $M_T/M_t = 0.65$ in Comerón et al. (2012) and $M_T/M_t = 0.77$ here after using Equation 5 in Comerón et al. (2011a). We could use a gas disc surface density larger than 20% of that of the thin disc to reflect the fact that the gas mass is $\sim 45\%$ that of the thin disc (Table 2). However, this would not take into account that usually gas discs are more extended than stellar discs. Furthermore, when we refitted the luminosity profiles with double the gas surface density, we obtained the same M_T/M_t within 1%.

We find that 90% of the light coming from the region $|z| \gtrsim 5''$ ($z \gtrsim 970 \text{ pc}$) is emitted by the thick disc. From now on we

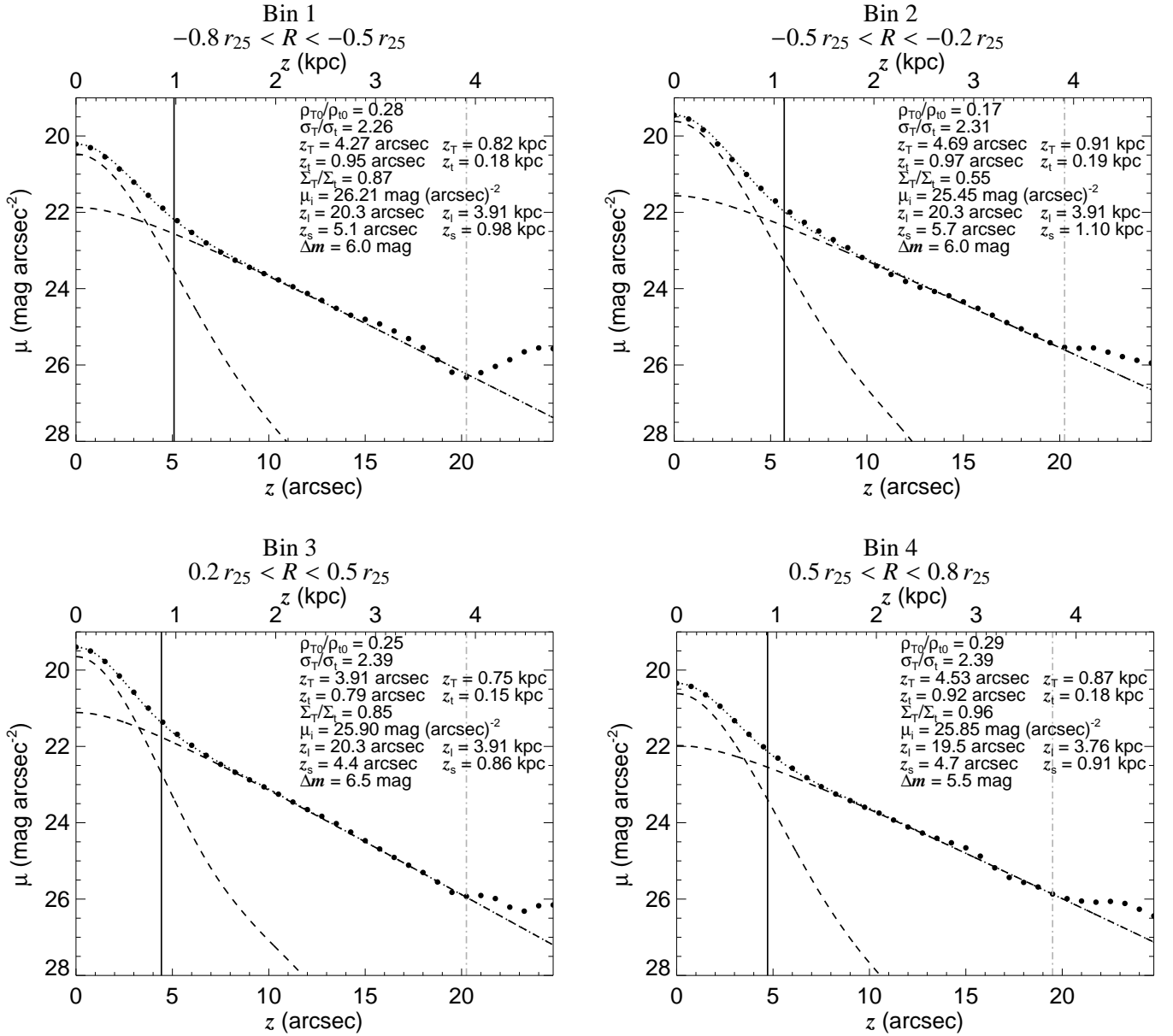


Fig. 2. Luminosity profiles of ESO 533-4 in the four bins perpendicular to the mid-plane that are indicated in Figure 1 (large dots). The fits are indicated by the dotted lines and the contribution of the thin and the thick discs are indicated by dashed lines. The vertical solid line indicates the height, z_s , above which 90% of the light comes from the thick disc according to our fit. The dot-dash grey vertical line indicates the maximum height, z_t , that we use for the fit. ρ_{T0}/ρ_{10} stands for the thick/thin disc mass density ratio at the mid-plane, σ_T/σ_t for their velocity dispersion ratio, z_T and z_t for the thick and thin disc vertical scale-heights, Σ_T/Σ_t for the thick to thin disc mass ratio, μ_i for the lowest fitted surface brightness level, and Δm for the range in magnitudes over which the fit was done.

consider that region as that where the thick disc dominates the surface brightness.

From our fits, we obtain that 39% of the light comes from the thick disc. In Salo et al. (2015) this fraction is 33% when using GALFIT3.0 (Peng et al. 2010) for the decomposition (GALFIT3.0, though performing a simultaneous 2D fit over the whole galaxy, oversimplifies the luminosity profiles perpendicular to the mid-planes by assuming that the discs have vertical $\text{sech}^2(z/z_0)$ profiles). The GALFIT3.0 thick disc scale-height is slightly underestimated ($z_T = 3''.4$ for GALFIT3.0 versus $z_T = 4''.4$ in our determination when averaging over the four fits in Figure 2). GALFIT3.0

finds that the height above which 90% of the light comes from the thick disc is $z = 4''.6$.

3. Observations

The spectroscopic observations were made on the nights 6 – 7 and 7 – 8 of August 2013. We used the integral field unit mode of VIMOS with the High Resolution Blue grism and a spatial resolution of $0''.66 \times 0''.66$ per fibre. The FOV of this mode is $27'' \times 27''$. The wavelength coverage of this configuration is 3700 – 5350 Å and the dispersion is $0.71 \text{ Å pixel}^{-1}$.

The total in-target exposure was 6.5 hours (2 hours in the first night and 4.5 hours during the second night). The exposure was divided into 13 observing blocks (OBs) with a few arcsecond dithering between them. Each OB exposed ESO 533-4 for 30 minutes. We also took 4 minute exposures of the sky, at a $2'$ distance in the direction perpendicular to the mid-plane. During the first night, a sky exposure was taken for every two galaxy OBs. During the second night two sky exposures were taken for every three galaxy OBs. Both nights were photometric and dark. The seeing was large ($\gtrsim 1''$), but this does not affect our science because in any case we need a large spatial binning to study the thick disc with a sufficiently large signal-to-noise ratio (S/N).

Standard calibration exposures (flat fields, bias, calibration lamps) and spectrophotometric standard stars were taken for the two nights.

4. Data reduction

4.1. Basic reduction

First, we used IDL's `LA_COSMIC` routine to clean the cosmic rays.

The spectra were reduced and flux calibrated by the VIMOS pipeline. The Reflex environment (Freudling et al. 2013) was used to run the pipeline. VIMOS has four quadrants and the pipeline provides independent reductions for each quadrant. Therefore, the output of the initial reduction was $4 \times 13 = 52$ sets of spectra corresponding to the galaxy.

For each of the quadrants of the sky exposures, we created a single spectrum by averaging the spectra in each spaxel with a 3σ clipping. We calculated the sky emission for each of our galaxy exposures, by associating them to the average of the sky spectra from the same quadrant taken within 64 minutes. This time was set so at least one sky exposure could be linked to each galaxy exposure, but in some cases there were up to four. Each of the quadrants has a remarkably uniform sky background. The quadrant number 2 has $\sim 40\%$ less signal than the others.

The information in headers could not be used for spacial alignment due to few arcsecond imprecisions in the pointing. To circumvent this problem, we tried to align the frames by finding point sources in images made by collapsing the spectra. However, the two point sources in the vicinity of the pointings were close to the edge of the field, and thus did not show up in some of the exposures due to the ditherings. Then, we built [OIII] images by integrating in the spectral direction from $\lambda = 5047.5 \text{ \AA}$ to $\lambda = 5054.6 \text{ \AA}$ (this takes into account the redshift of ESO 533-4). Unresolved star-forming regions stand out in the [OIII] images and were used for manual alignment. Once the galaxy frames were spacially aligned, we summed the spectra for every spaxel using a 3σ clipping. We also summed for each spaxel the sky spectra associated to the galaxy frames that were not clipped away. For every wavelength in each spectrum corresponding to each spaxel, we estimated the S/N by considering the Poisson noise and the readout noise,

$$S/N = \frac{S_{\text{galaxy}}}{\sqrt{S_{\text{galaxy}} + S_{\text{sky}} + \sum_i (RON_i)^2}} \quad (1)$$

where, S_{galaxy} is the signal from the galaxy, S_{sky} is the signal from the sky, and RON_i are the read-out noises of each of the exposures that were summed to obtain the final spectrum of a given spaxel. We neglected the dark current contribution to the

S/N because it is very small (typically $5 e^- \text{ hr}^{-1} \text{ pix}^{-1}$ according to the VIMOS Pipeline User Manual¹).

We masked the two point-sources in the field, thought to be foreground stars or ESO 533-4 globular clusters, as well as several spaxels in the edges that were covered by few exposures. The two point-sources in the field were used to align the IFU data with the S^4G data. The alignment precision is estimated to be of the order of $1''$.

4.2. Kinematics

4.2.1. Velocity maps

Spacial binning is necessary to achieve a S/N good enough to study thick disc kinematics. The binning was done with the Voronoi binning code by Cappellari & Copin (2003) with the condition of $S/N \sim 25$ for spectral pixels between $\lambda = 4500 \text{ \AA}$ and $\lambda = 5000 \text{ \AA}$.

To find the velocity field of ESO 533-4 we fitted the spacially binned spectra with the MILES stellar population synthesis models (Vazdekis et al. 2010) using the penalized pixel-fitting (pPXF) code by Cappellari & Emsellem (2004)². It is usually required to Gauss-convolve either the library or the observed spectra so their FWHMs match. However, we found that the FWHM in our spectra is $\Delta\lambda \approx 2.2 \text{ \AA}$ on the blue side and $\Delta\lambda \approx 2.8 \text{ \AA}$ on the red side, which is very similar to MILES' FWHM, $\Delta\lambda = (2.51 \pm 0.07) \text{ \AA}$. We therefore decided not to make a convolution. Because of the relatively low S/N of the bins, we only fitted two momenta. Emission lines were masked with a mask $\Delta v = 1000 \text{ km s}^{-1}$ in width. We used an eight degree additive Legendre polynomial to correct the continuum shape for dust reddening and possible photometric calibration problems. The velocity map is shown in the right panel in Figure 3. The height above which 90% of the light comes from the thick disc is $|z| \approx 5''$. Therefore, the uppermost and the lowermost rows of bins should be dominated by the thick disc light.

4.2.2. Rotation curves

We made rotation curves of ESO 533-4 at five different heights, namely $z = 0$, $z = \pm 3''$ ($\sim 0.6 \text{ kpc}$), and $z = \pm 8''$ ($\sim 1.5 \text{ kpc}$; Figure 4). The $z = \pm 8''$ cuts should be well within the region where the light emission comes mostly from the thick disc. The profiles take into account the movement of the Earth away of the galaxy ($\sim 19 \text{ km s}^{-1}$ at the time of the year at which the observations were made) and assume a heliocentric systemic velocity $v_{\text{sys}} = 2596 \text{ km s}^{-1}$ (Table 2). The points in the rotation curves are calculated by making axial cuts in the data used for Figure 3. The error bars in the rotation curves are estimated by producing 20 Monte-Carlo simulations (with the estimated noise for each pixel) when obtaining the kinematics from each spectrum.

When extrapolated to $R = 0$, the rotation curves are close to $V = 0$, which confirms that the spectra calibration process is robust. It is also reassuring that our $z = 0$ rotation curve matches very well with the $H\alpha$ rotation curve from Mathewson et al. (1992) once this has been offset by $+10 \text{ km s}^{-1}$. The correction seems necessary because taken as it is published, the velocity at $R = 0$ is about -10 km s^{-1} . If the offset is not made, the maximum in the $H\alpha$ rotation curve is found at $v \sim 160 \text{ km s}^{-1}$ on the

¹ <ftp://ftp.eso.org/pub/dfs/pipelines/vimos/vimos-pipeline-manual-6.8.pdf>

² Both pPXF and the Voronoi tessellation codes can be found at <http://www-astro.physics.ox.ac.uk/~mxc/software/>

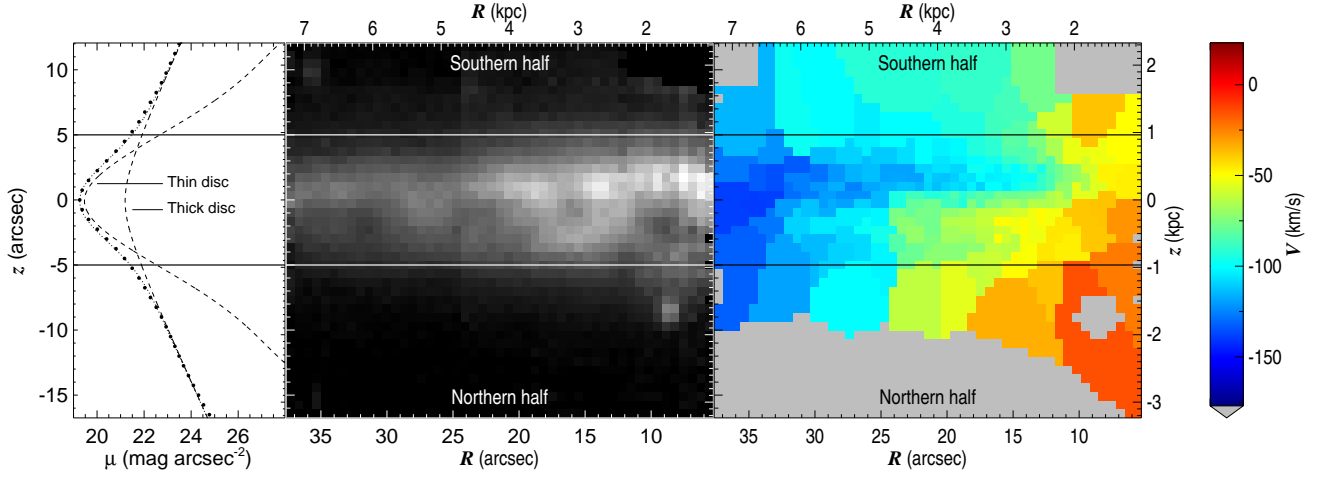


Fig. 3. Left panel: Symmetrized mid-infrared S^4G luminosity profile and thin/thick disc decomposition of the $0.08r_{25} - 0.69r_{25}$ ($0.8 - 7.3$ kpc) axial range of ESO 533-4 (the one covered by the IFU). The horizontal solid lines indicate the height, z_s above which 90% of the light comes from the thick disc. Middle panel: image of the observed field made by collapsing the spectra. Right: velocity field of ESO 533-4 after the subtraction of the recession velocity. The horizontal axis indicates the axial distance to the galaxy centre and the vertical axis indicates the distance from the mid-plane.

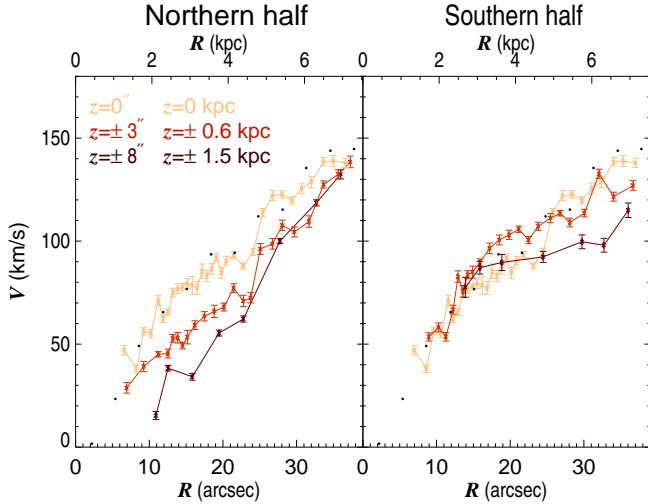


Fig. 4. Rotation curves of ESO 533-4 at different heights as indicated by the colours. The Northern half of the disc corresponds to the bottom half of the disc in Figure 3. The black dots correspond to the Mathewson et al. (1992) $H\alpha$ rotation curve with a $+10$ km s⁻¹ offset (see text).

Western side of the galaxy and at $v \sim 140$ km s⁻¹ on the Eastern side, which would be strange in an undisturbed canonical rotation curve. We suspect an inaccurate calibration or heliocentric correction to be the source of the problems with the $H\alpha$ data as published.

4.3. Stellar populations

To study the stellar populations, we manually created new spacial bins by combining those used in the velocity map. Before summing all the spectra from the low- S/N bins to create the high- S/N binning, we shifted their wavelengths so they all corresponded to a 2500 km s⁻¹ recession velocity. We made the bins roughly rectangular, with the long side in the direction of the

plane of the galaxy, so different heights could be studied. In order to achieve the required S/N for the thick disc, we summed the light from the two sides of the mid-plane. Manual binning is essential because the Voronoi tessellation tries to make “compact” or “round” bins (Cappellari & Copin 2003). This second binning yielded spectra with a $S/N \sim 80$ in the $\lambda = 4500$ Å to $\lambda = 5000$ Å spectral range.

To obtain the stellar population map, the spectra were again fitted using pPXF with a regularization factor of 200. The regularization factor is used to smooth the stellar populations. The continuum was corrected with multiplicative Legendre polynomials (for details on the regularization and the use of Legendre corrective polynomials see the pPXF documentation). These corrections are essential because of the dust reddening close to the mid-plane and because the blue side of the spectrum has little signal, so it is prone to photometric calibration errors. We tested which polynomial order would work best for our observations. The thick disc fit, where dust reddening is likely to be negligible, is very stable with respect to changes of the order of the polynomial (which indicates little dust affecting the spectra and also a good data calibration that makes correcting polynomials unnecessary). The fitted thin disc stellar populations are very dependent of the order for orders smaller than ~ 10 . For larger orders the fitted stellar populations change little with changes in order, which probably indicates that the continuum shape is properly corrected for differential dust absorption and no further orders are required. The results presented here are fitted with an order 14 polynomial, which is comparable to what others have used with VIMOS data (for example Chilingarian et al. 2009, used 18). The stellar population map is presented in Fig. 5. The fit to the spectra in two of our tessels are shown as an example in Figure 6. In Figure 7, mean age and metallicity maps are shown.

5. Interpretation of the data

5.1. Kinematics

We find an asymmetry in the velocity map: within the thin disc at a given radius, the Southern (upper) half of the galaxy seems

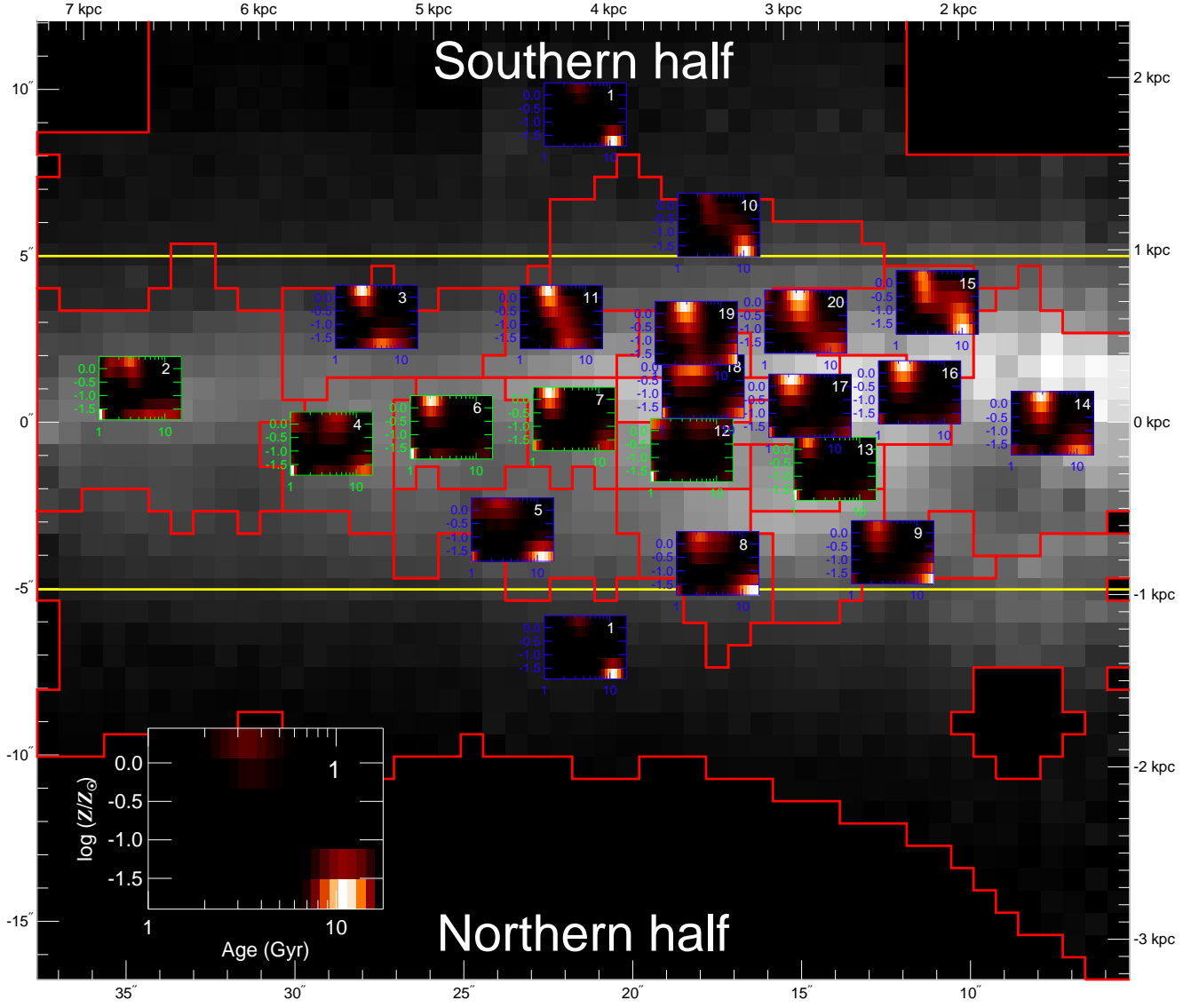


Fig. 5. Stellar populations of ESO 533-4. The background image is the same as in the middle panel in Figure 3. The red lines indicate the spacial bins used for the analysis. The horizontal solid yellow lines indicate the height above which 90% of the light comes from the thick disc. On top of each bin there is a stellar population plot with the horizontal axis corresponding to the ages in Gyr and the vertical axis corresponding to the metallicities in $\log(Z/Z_{\odot})$. The two thick disc sections (uppermost and lowermost tessels) were actually treated as a single bin. The colours in the plots for each bin indicate the mass fraction of a given stellar population. Plots with green axes correspond to those with at least a 10% mass fraction fitted to be in a young population with a low metallicity (see Section 5.2). The bottom-left corner of the figure shows an enlarged version of one of the stellar population distributions to improve the readability of the axes.

to rotate faster than the Northern (lower) half (Figure 3 and the $z = \pm 3''$ or $z = \pm 0.6$ kpc rotation curves in Figure 4). Possible reasons for the asymmetry are the presence of a dust lane in a not perfectly edge-on disc and features which are not symmetric with respect to the mid-plane (e.g., some phases of a buckling bar such as those seen in Martínez-Valpuesta et al. 2006). The latter possibility, however, is unlikely because there is no sign of a strong bar in ESO 533-4 (boxy/peanut inner isophotes; Combes & Sanders 1981).

The rotation curves for the Northern half of the galaxy (below the mid-plane in Figure 3) decrease monotonically in amplitude as z increases. For the Southern half, this is only true for

$R \gtrsim 25''$ (a striking feature of the rotation curves is that for the Southern half of the galaxy, we find the velocities at $z = 3''$ to be larger than those at $z = 0$ in the $12'' - 25''$ or $2.3 - 4.8$ kpc axial extent). The difference in velocities between the mid-plane and $|z| = 8''$ ($z = \pm 1.5$ kpc) is $10 - 30 \text{ km s}^{-1}$ at the radius where the maximum circular velocity is reached. The apparent rotational lag of the thick disc must at least partly be a consequence of a stronger asymmetric drift caused by the larger velocity dispersion of the thick disc. Part of the lag might be caused by the presence of counterrotating stars. Finally, part of the apparent lag might be due to the fact that we may be looking at a not perfectly edge-on disc.

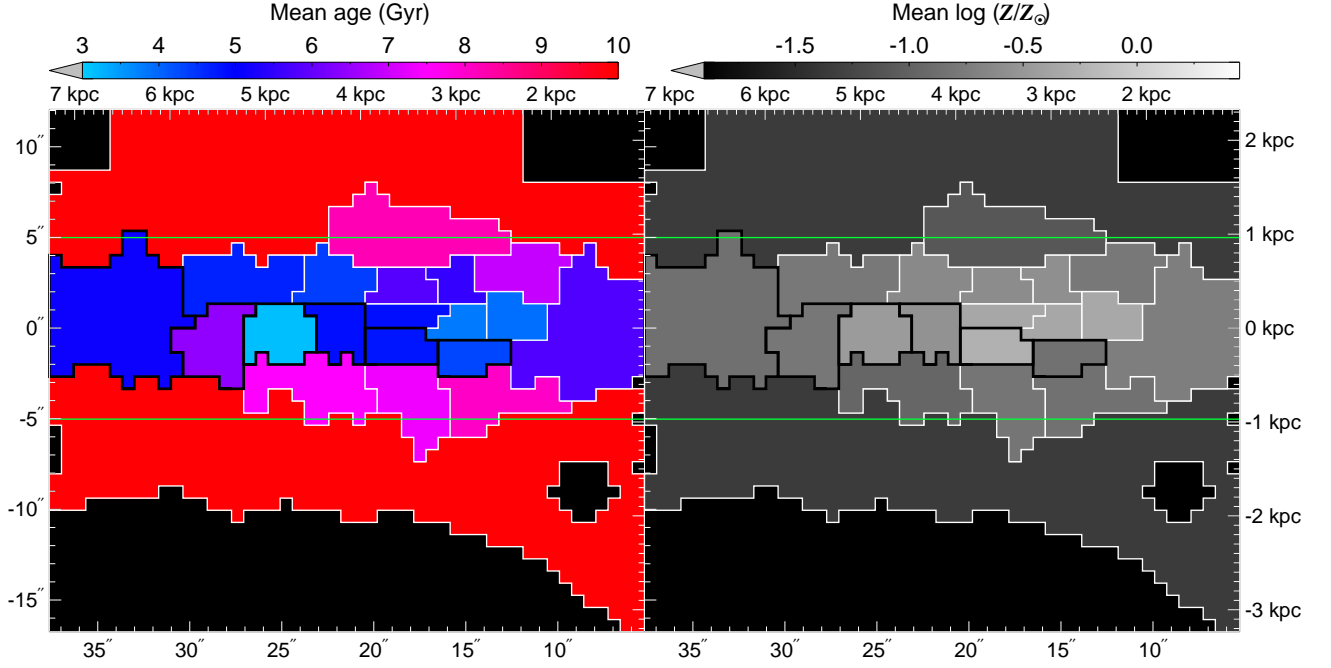


Fig. 7. Mean stellar age (left) and metallicity (right) maps. The white lines and black lines indicate the tessellation. Black lines surround tessels where at least a 10% of the mass fraction is fitted to be in a young population with a low metallicity. The horizontal solid green lines indicate the height above which 90% of the light comes from the thick disc.

To check for the causes of the asymmetries in the velocity map and for those of the lag of the thick disc, we run a set of models using GADGET-2 (Springel 2005). The initial models were created with the GalactICS software (Kuijken & Dubinski 1995). They included a thin disc and a thick disc. Both had similar scale-lengths. The scale-height of the thick disc was ~ 4.9 times larger than that of the thin disc and the mass ratio was 1.1/1.5 in agreement with the values in Table 2 and the fits in Figure 2. Each of the discs was made of 1.03×10^6 particles and a Toomre parameter $Q = 1.3$. We also included a small spherical CMC with a mass fifty times smaller than that of the sum of the two discs. It was made of 2×10^4 particles. Finally, we embedded the whole system into a dark matter halo made of 1.08×10^6 particles. The distribution of dark matter particles was set to make a roughly flat rotation curve at large radii. At a radius of two scale-lengths the disc contributed to about 40% of the total radial force. The baryonic mass of our model scaled to the observed axial and vertical (Figure 9) profiles and the rotational velocity amplitude is $2.9 \times 10^{10} M_{\odot}$. This is close to the actual mass of ESO 533-4. Models with different dark matter fractions could be created, but then having a good simultaneous vertical and axial match between the models and the observations would not have been possible. The model snapshots shown here are for models that have been run for over ten rotations at all the radii covered by the VIMOS observations. This guarantees that the thin and the thick discs have settled to equilibrium.

To account for the effect of dust, we assumed it to follow the distribution of thin disc stars except for the fact that we consider a three times smaller scale-height. The ratio of three is because we assumed dust to be mixed with dense gas. In the Milky Way dense gas has a scale-height of ~ 100 pc (Langer et al. 2014) whereas the thin disc scale-height is ~ 300 pc (Gilmore & Reid 1983). We assumed the dust to cause a grey absorption. We studied several dust densities. The results shown here correspond to

an optical depth of $\tau = 8$ to the centre of the galaxy when looking at it from a perfectly edge-on view.

We checked whether ESO 533-4 has some measurable deviation from an edge-on orientation by looking at its colour map (Figure 8). We found the redder sections of the thin disc to lie slightly below the mid-plane ($\sim 1''$). This implies that the near side of the galaxy is the top one, which corresponds to the Southern side of the observed galaxy in Figure 3. We find that a $\sim 1''$ deviation of the dust lane corresponds to a galaxy inclination $i \approx 85^\circ$ in our models (we simulated colour maps by comparing the luminosity profiles of models with and without dust). ESO 533-4's inclination, however, is likely to be closer to 90° given the extremely thin aspect of the disc and the lack of evidence for spiral features (Figure 1). If the dust distribution were less centrally concentrated than in our models, deviations of only $2-3^\circ$ away from edge-on would be enough to explain the vertical shift of the dust lane. Clear examples of galaxies where the dust distribution is more extended than that of the stellar disc are known (e.g., the Sombrero Galaxy or the system studied in Holwerda et al. 2009).

To create synthetic velocity maps, we assigned the MILES spectrum of a 2.5 Gyr star with solar metallicity to thin disc particles. For the thick disc we used the spectrum of a 10 Gyr star with metallicity $Z = 0.2 Z_{\odot}$. We created synthetic images of the galaxy by projecting them and convolving them with a Gaussian PSF with a FWHM of $1''.2$. We then used the Voronoi tessellation software to create a tessellation matching the one obtained for the VIMOS data (i.e., the density of tessels in the thin disc is similar). We then obtained the velocity maps exactly as we did for the VIMOS data.

Figure 10 shows the velocity maps for several models in an area approximately matching that of the VIMOS observations. The top row in the figure corresponds to galaxies with no dust and the bottom row corresponds to galaxies with dust. Models with no dust are symmetric with respect to the mid-

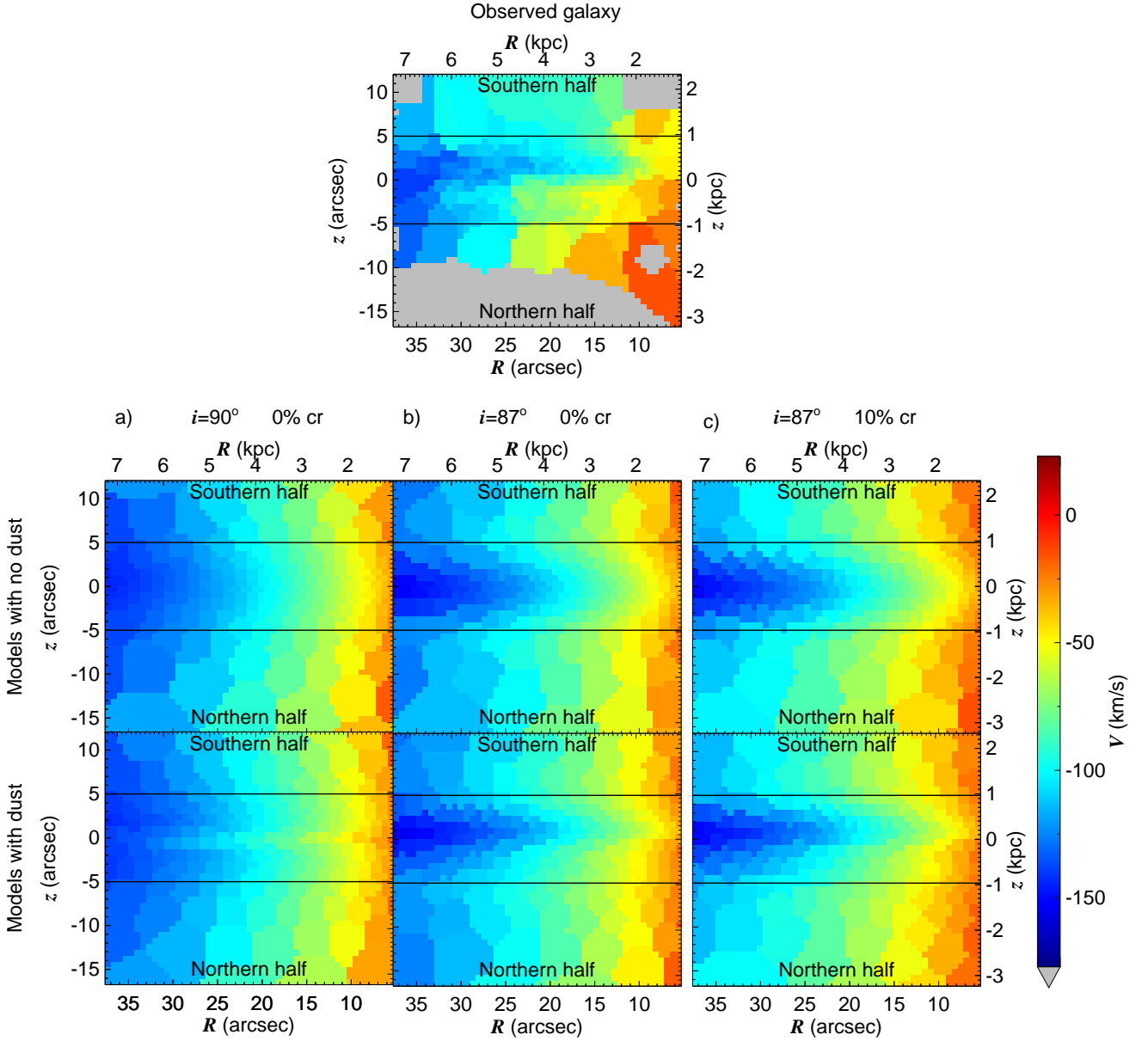


Fig. 10. Top: observed velocity map of ESO 533-4. Middle and bottom rows: set of velocity maps from models designed to mimic the region shown in Figure 3. The three columns correspond to a) a perfectly edge-on galaxy with no counterrotating material, b) a galaxy 3° away from edge-on with no counterrotating material, and c) a galaxy 3° away from edge-on with 10% of counterrotating material in the thick disc. The top row corresponds to models with no dust and the bottom row corresponds to models with some amount of dust (see text). The horizontal lines indicate the height above which $\sim 90\%$ of the light comes from the thick disc.

plane. Models with dust, when not seen exactly edge-on, have some degree of asymmetry.

The left column in Figure 10 correspond to models with a perfectly edge-on view of the galaxy. The optical depth is the largest close to the mid-plane. Dust attenuates the light from the point which is closer to the galactic centre (that with the largest velocity along the line of sight) more than that of stars closer to the observer. Thus, the dust attenuation causes an apparent slowing of the stars around $z = 0$.

The middle and the right columns in Figure 10 show that dust is able to create asymmetries when looking at galaxies that are not perfectly edge-on (inclination $i = 87^\circ$ in the example shown here). The larger attenuation on one side of the galaxy causes the asymmetry in the velocity maps: the maximum ve-

locity at a given radius is not found at the mid-plane, but slightly above it. The deviations from symmetry in our models with $i = 87^\circ$ and dust are in qualitative agreement with the observations (Figure 3).

To find the cause of the apparent lag in the thick disc of ESO 533-4 (asymmetric drift, galaxy inclination, and/or presence of counterrotating stars), we created rotation curves at different heights for the models in the same way we did for the VIMOS data (Figure 11). We find that at the radius where $v(z = 0) \approx 150 \text{ km s}^{-1}$, the difference in velocity between the mid-plane and $z = \pm 8''$ ($z = \pm 1.5 \text{ kpc}$) is $\sim 20 \text{ km s}^{-1}$ for a model with no counterrotating material and $\sim 30 \text{ km s}^{-1}$ for a galaxy whose thick disc has a 10% of counterrotating material. These numbers are similar to those observed in ESO 533-4 and

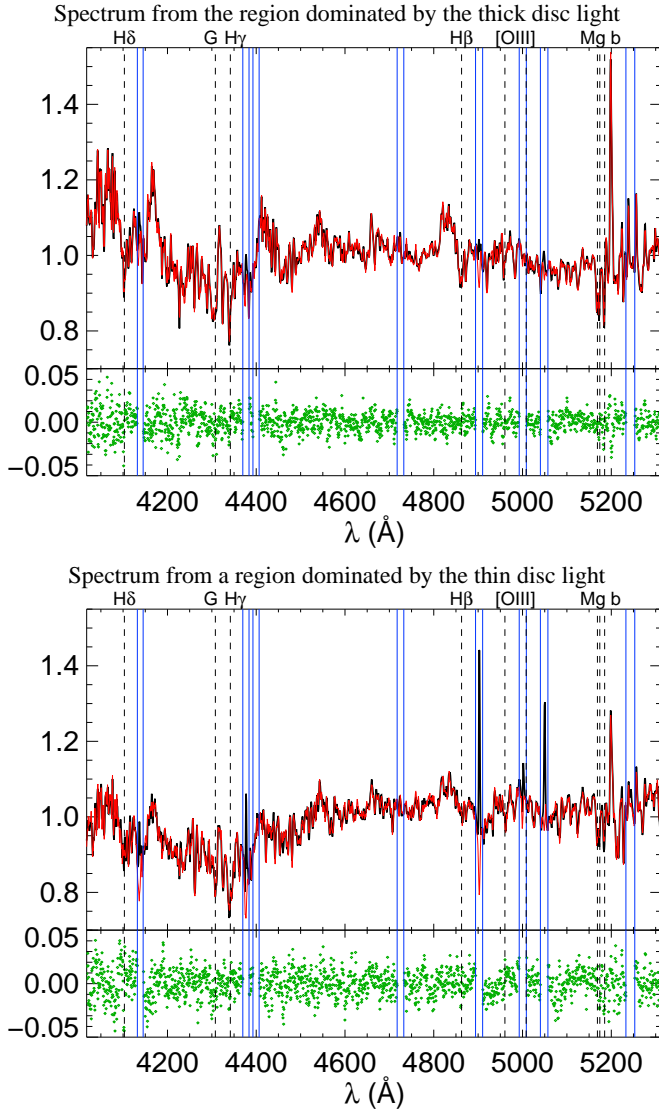


Fig. 6. Two examples of rest-frame spectra obtained from our $S/N \sim 80$ tessellation. The black line corresponds to the actual spectrum, the red line corresponds to the fit, and the blue vertical lines indicate the spectral windows that were masked because of the possible presence of emission lines. Residuals are shown with green symbols below the spectra. The top spectrum belongs to the thick disc dominated region and the bottom spectrum to the rightmost thin disc dominated tessell in Figure 5. The spectra are normalized to their median value. Several spectral lines are indicated with dashed lines.

indicate that the thick disc has little or no counterrotating material. The effect of the asymmetric drift plus the disc orientation (slightly away from edge-on) are enough to explain the thick disc lag.

In Figure 11 we see how, in the Southern half, the $z = 3''$ ($z = \pm 0.6$ kpc) curve overlaps with that at $z = 0$ for some radial extent. This is because dust absorption is larger at $z = 0$ than at $z = 3''$. By increasing dust absorption it is possible to get the $z = 3''$ curve above the $z = 0$ curve for some axial extent just as in the observations. This effect is therefore most likely due to dust.

Our models are not able to reproduce that the rotation curves of the Northern half of ESO 533-4 for $R < 25''$ ($R < 4.8$ kpc)

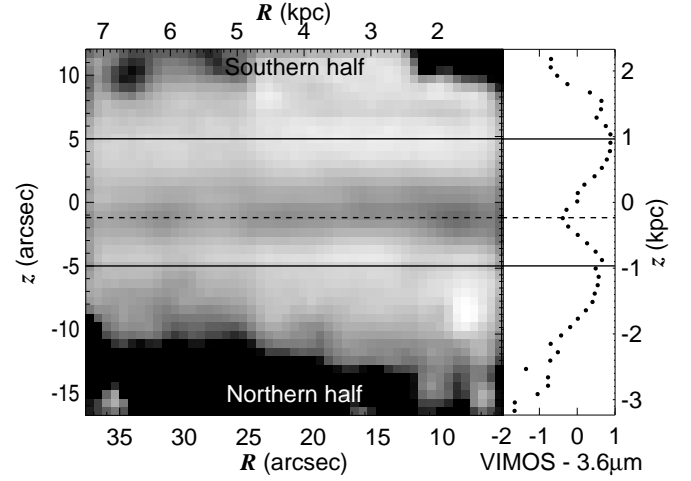


Fig. 8. Left: VIMOS-3.6 μ m colour map. The VIMOS image was degraded to the S^4G resolution. Right: median VIMOS-3.6 μ m as a function of the height with an arbitrary zero point. The solid horizontal lines indicate the height above which $\sim 90\%$ of the light comes from the thick disc. The dashed horizontal line indicates the reddest height within the thin disc dominated region.

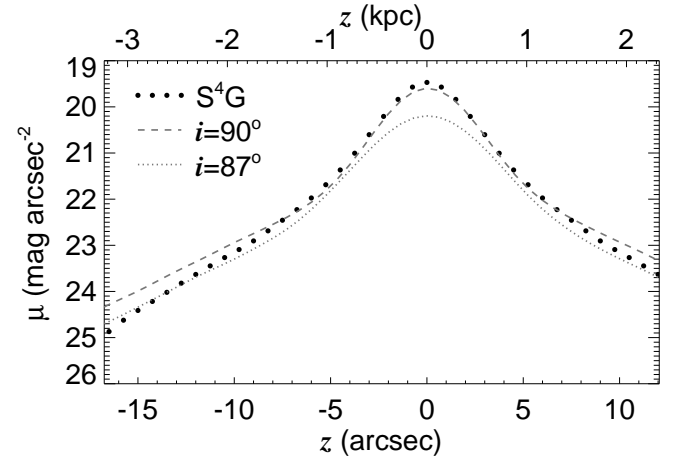


Fig. 9. Luminosity profiles of the observed galaxy (large black dots) and the model galaxies (grey lines) in the $0.08r_{25} - 0.69r_{25}$ axial range (dust extinction set to zero). Two models, one with $i = 90^\circ$ (dash), and one with $i = 87^\circ$ (dots), are shown. The zero point of the model profiles is arbitrary.

where the thick disc lags by 30 km s^{-1} or more with respect to the mid-plane. The mismatch between the thick disc and the $z = 0$ rotation curves could be due to some fraction of counterrotating stars in the inner parts of the galaxy. However, if that were the case it would be difficult to explain why the counterrotating material shows up only in one side of the galaxy.

5.2. Stellar populations

We can distinguish three distinct stellar populations in the subplots in Figure 5:

- An old (~ 10 Gyr) metal-poor population.

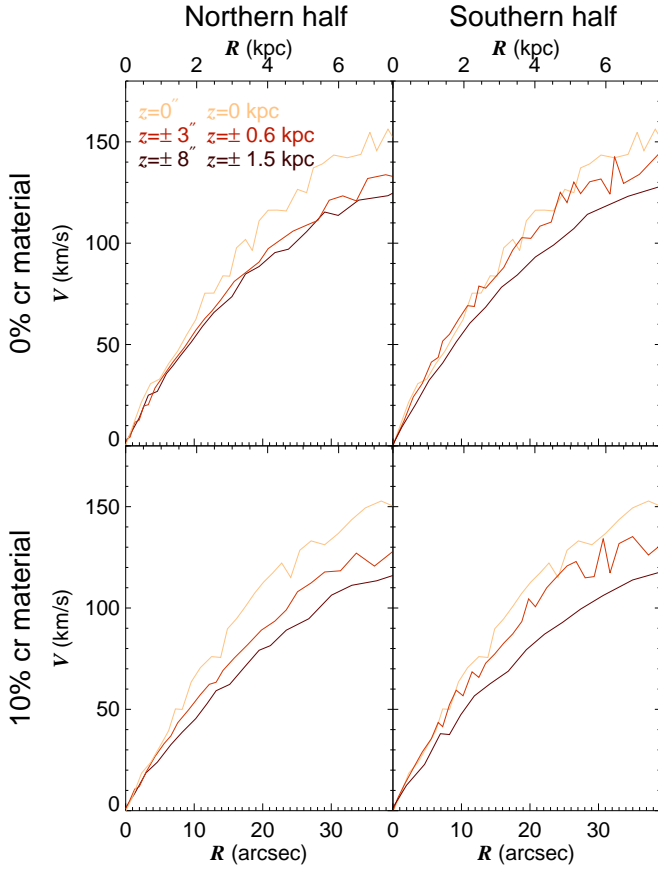


Fig. 11. Rotation curves of models at different heights as indicated by the colours. The Northern half of the disc corresponds to the bottom half of the disc in Figure 10. The top row rotation curves correspond to a model with $i = 87^\circ$, dust, and 0% of counterrotating material and the bottom row corresponds to similar model but with 10% of counterrotating material in the thick disc.

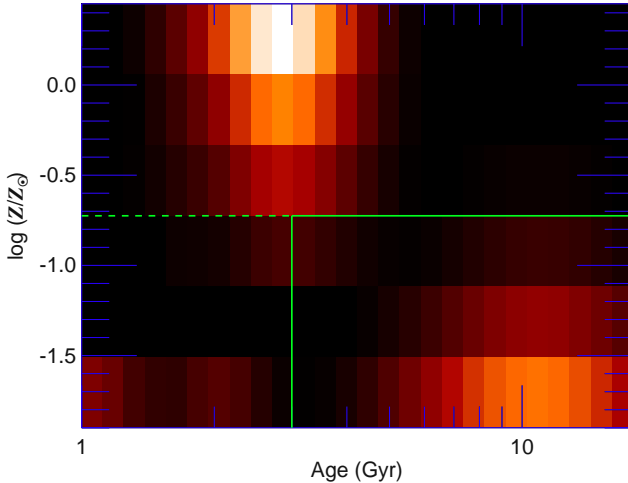


Fig. 12. One of the subplots in Figure 5 (the rightmost). The green lines indicate the divisions between the thick disc population (bottom right), the metal-rich thin disc (top), and the metal-poor thin disc (bottom left).

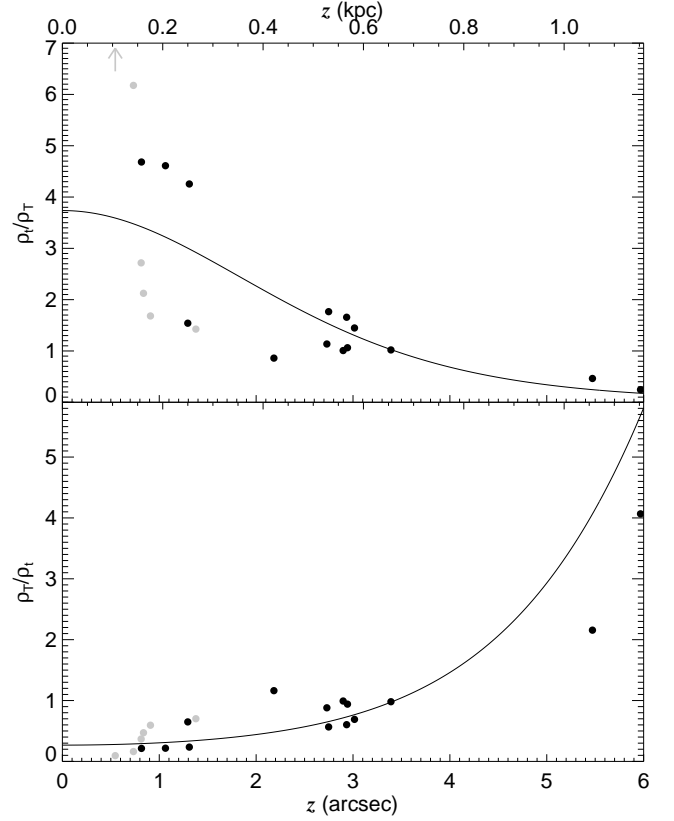


Fig. 13. Ratio between the masses of the thin and thick disc stellar populations (top panel) and its inverse (bottom panel), as a function of the height $|z|$ of the Figure 5 tessell. The lines indicate the same ratios according to the fit to the light profiles (Figure 3). Grey points indicate the tessels where the metal-poor young population is fitted to be more than 10% of the mass. The arrow in the top panel indicates an outlier with a value $\rho_t/\rho_T = 10.5$.

- A relatively young metal-rich population.
- In some fits we also find a young metal-poor population.

To quantify the fraction of mass associated with each of these three stellar populations in each tessell, we divided the diagrams in three regions as seen in Figure 12. The limit between metal-rich and metal-poor populations is set at $\log(Z/Z_\odot) = -0.7$. We set the limit between the young and old metal-poor populations at $t = 3$ Gyr. While a $t = 3$ Gyr stellar population is young compared to what one would expect for a thick disc population, the regularization made by pPXF causes stellar populations with peak ages at $t \sim 10$ Gyr to extend down to smaller ages. This is not a problem, because the peak of the young metal-poor population is very narrow and centered at $t = 1$ Gyr.

The first of the populations in the list is naturally associated to the thick disc, and the second one is likely to be related to the thin disc. To further confirm this, we find the old metal-poor population to dominate the mass budget in the bin with the largest height, whereas the younger metal-rich population dominates close to the mid-plane. In many tessels the stellar population fits show that the thin and the thick disc populations are well separated in the Age – $\log(Z/Z_\odot)$ plane, i.e., there is no transition between the two. In these tessels, the thin and the thick disc stars seem to belong to two distinct populations. In other tessels (10, 11, 15, and 20 in Figure 5) the two populations are not so

clearly separated, but there are still two clear maxima that would correspond to the two disc populations. In those tessels, the continuity between the two populations might be a consequence of the smoothing introduced by the regularization.

The third population (young and metal-poor) is not expected in the galaxy formation and evolution scenarii unless it is located in the metal-poor outskirts of the disc. However, for several tessels this population is fitted to be responsible for 10% or more of the stellar mass, so those stars are unlikely to belong to the extended but very low density outskirts of a disc. We found that the tessels where more than 10% of the mass belongs to that population lie at or slightly below (North) the mid-plane. This is the region where the dust layer is affecting the most the kinematical map of the galaxy (see Figure 8 and the discussion in Section 5.1). It is therefore likely that this population is an artefact due to dust absorption. Indeed, even though pPXF is supposed to handle differential dust absorption with the multiplication of the input spectra with Legendre polynomials, we applied the code where the dust absorption can be several magnitudes.

In what follows we will consider the metal-poor young population as part of the thin disc population. If we assume that the stars are divided into a thin and a thick disc population (as indicated by many of the $\text{Age} - \log(Z/Z_\odot)$ plots in Figure 5), we can test the assumptions made when fitting the luminosity profiles to decompose them into the thin and thick disc components as made in Comerón et al. (2011b,a, 2012, 2014). We calculated for each tessel the mass that corresponds to the thin and the thick discs according to the fit in the left panel of Figure 3. To do so, we weighted the spaxels accounting both for the vertical and the axial luminosity profiles (axial luminosity profile from Comerón et al. 2012). As seen in Figure 13 the agreement between the results obtained from the stellar population maps and that from our thin/thick disc modelling is very good, especially if we take into account the uncertainties and assumptions made in the modelling process.

6. Summary of the results, discussion and conclusions

The main findings presented in this Paper are:

- The velocity field of ESO 533-4 is compatible with that of a galaxy inclined a few degrees from edge-on with a significant dust absorption in the equatorial plane. The near side of the galaxy is the Southern one.
- The apparent velocity lag of the thick disc can be explained by asymmetric drift and because of the projection effects arising from studying a disc a few degrees ($2 - 3^\circ$) away from edge-on. Little or no counterrotating stars are needed to account for the asymmetric drift of the thick disc.
- The thick disc is made of old (~ 10 Gyr) and metal-poor stars. The thin disc is made of younger metal-rich stars. The two populations are differentiated in the $\text{Age} - \log(Z/Z_\odot)$ plane for the majority of the regions of ESO 533-4 studied in this Paper, with little evidence for a continuity between them. In the few regions (4 out of 20) where there is a continuity between the two populations, there are still two clear peaks that correspond to an old metal-poor population and a relatively young metal-rich population. This indicates that the stellar populations of the thin and the thick discs may be distinct.
- A third population of metal-poor young stars is seen in some sectors of the galaxy. These regions are the same where dust

absorption is the largest. This population is probably an artefact caused by the difficulties of handling extreme dust absorptions.

- The relative fractions of mass in the thin and the thick discs at different heights according to our stellar population analysis agree with those obtained from our thin/thick disc fits of mid-infrared luminosity profiles.

Let's first examine the lack of a significant fraction of counterrotating stars in the thick disc. If the thick disc stars were accreted in a succession of minor mergers, we would expect similar fractions of prograde and retrograde stars, unlike what we observe. If the thick discs were created in a few relatively major mergers (as in e.g. Read et al. 2008) or due to the fusion of a few protogalactic mergers as in Brook et al. (2004), there would be no guarantee that a particular galaxy would have counterrotating stars. Indeed, in the extreme case where only one such an event occurs, there is a 50% chance of having a prograde merger and a 50% chance of having a retrograde merger. Thus, the lack of counterrotating material in ESO-533-4 would not rule out a merger origin. If we consider the 1D spectroscopy study by Yoachim & Dalcanton (2008b) and our knowledge of the Milky Way kinematics (Chiba & Beers 2000), we find that none of the five massive galaxies ($v_c \gtrsim 120 \text{ km s}^{-1}$) for which thick disc kinematics are known has a counterrotating disc. Therefore, if all thick discs in high-mass galaxies share a similar history (which is a reasonable assumption, given that the ratio of the masses of the thin and thick discs are roughly similar for most of the high-mass galaxies; Comerón et al. 2014), a major merger origin is disfavoured by the currently available data. We thus tentatively propose that the thick disc of ESO 533-4 has formed either due to dynamical heating or that it was born dynamically hot in a turbulent disc with a large star formation rate.

To distinguish between those two mechanisms, we can use our stellar population data. We see that in most of the tessels in Figure 5 the thin and the thick disc populations are clearly differentiated in the $\text{Age} - \log(Z/Z_\odot)$ plane, which would go against a secular heating scenario where a continuous transition between the thin and the thick discs is expected. Instead, it would favour a scenario where the thick disc formed thick at high redshift in a relatively fast process. We however caution against over-interpreting the stellar population results because of the extremely dusty conditions under which the fitting is done. Confirmation of our stellar population results with longer wavelength spectra is thus desirable.

Another and probably more robust way to distinguish between the two mechanisms compatible with our kinematical data is hinted at in Minchev et al. (2015). In their model, age gradients naturally appear in the thick disc-dominated region. Such gradients would immediately confirm or infirm the formation scenario where discs are made at high redshift. Unfortunately, due to S/N constraints, we can only make a single bin out of all the thick disc dominated region, which prevents us from testing for the presence of an age gradient. Even if a larger number of thick disc bins could be made, the effect predicted by Minchev et al. (2015) would be very subtle because our observations extend only out to about 1.5 disc scale-lengths (Comerón et al. 2012), whereas large age difference (of the order of $2 - 4$ Gyr) would in theory be observed only over ranges of ~ 3 scale-lengths. Larger field of view observations (e.g., with MUSE) are thus needed to definitely settle this issue.

The conclusion is that, if we assume that all thick discs in high-mass galaxies share a common origin, observations favour a dynamical heating or turbulent disc origin for the thick disc in

ESO 533-4. A minor merger origin can be discarded, whereas a major merger origin is possible if a variety of scenarios is able to produce a thick disc in high-mass galaxies. The stellar population map of ESO 533-4 is affected by dust absorption and should be interpreted with caution. It seems to indicate that this particular galaxy has differentiated thin and thick disc stellar populations, as expected from a short event (either in an early turbulent disc or in a major merger). It thus seems to disfavour a secular evolution origin. A study of the axial gradients of the stellar ages in the thick disc is required to confirm this last assertion.

Acknowledgements. We thank our referee for helping to improve the interpretation of the data. We thank Dr. Valentin Ivanov for his help during a very complicated observing stint. We thank Dr. Julio Carballo-Bello for pointing out at some useful references. We thank Dr. Frédéric Bournaud for providing details about his simulations. This work is based on observations and archival data made with the Spitzer Space Telescope, which is operated by the Jet Propulsion Laboratory, California Institute of Technology under a contract with NASA. We are grateful to the dedicated staff at the Spitzer Science Center for their help and support in planning and execution of this Exploration Science program. We also gratefully acknowledge support from NASA JPL/Spitzer grant RSA 1374189 provided for the S⁴G project. This research has made use of SAOImage DS9, developed by Smithsonian Astrophysical Observatory. This research has made use of the NASA/IPAC Extragalactic Database (NED) which is operated by the Jet Propulsion Laboratory, California Institute of Technology, under contract with the National Aeronautics and Space Administration. We acknowledge the usage of the HyperLeda database (<http://leda.univ-lyon1.fr>). SC, HS, and EL acknowledge support from the Academy of Finland. JJ thanks the ARC for financial support via DP130100388, the authors acknowledge support for the FP7 Marie Curie Actions of the European Commission, via the Initial Training Network DAGAL under REA grant agreement number 289313.

References

- Abadi, M. G., Navarro, J. F., Steinmetz, M., & Eke, V. R. 2003, *ApJ*, 597, 21
- Ade, P. A. R., Aghanim, N., Arnaud, M., et al. 2015, *ArXiv e-prints*
- Alpher, R. A. & Herman, R. C. 1949, *Physical Review*, 75, 1089
- Athanassoula, E. 2013, Bars and secular evolution in disk galaxies: Theoretical input, ed. J. Falcón-Barroso & J. H. Knapen, 305
- Bournaud, F., Elmegreen, B. G., & Martig, M. 2009, *ApJ*, 707, L1
- Bournaud, F., Perret, V., Renaud, F., et al. 2014, *ApJ*, 780, 57
- Brook, C. B., Kawata, D., Gibson, B. K., & Freeman, K. C. 2004, *ApJ*, 612, 894
- Burstein, D. 1979, *ApJ*, 234, 829
- Buta, R. J., Sheth, K., Athanassoula, E., et al. 2015, *ApJS*, 217, 32
- Cappellari, M. & Copin, Y. 2003, *MNRAS*, 342, 345
- Cappellari, M. & Emsellem, E. 2004, *PASP*, 116, 138
- Chiba, M. & Beers, T. C. 2000, *AJ*, 119, 2843
- Chilingarian, I. V., De Rijcke, S., & Buyle, P. 2009, *ApJ*, 697, L111
- Combes, F. & Sanders, R. H. 1981, *A&A*, 96, 164
- Comerón, S., Elmegreen, B. G., Knapen, J. H., et al. 2011a, *ApJ*, 741, 28
- Comerón, S., Elmegreen, B. G., Knapen, J. H., et al. 2011b, *ApJ*, 738, L17
- Comerón, S., Elmegreen, B. G., Salo, H., et al. 2012, *ApJ*, 759, 98
- Comerón, S., Elmegreen, B. G., Salo, H., et al. 2014, *A&A*, 571, A58
- Comerón, S., Knapen, J. H., Sheth, K., et al. 2011c, *ApJ*, 729, 18
- Curtis, H. D. 1917, *PASP*, 29, 206
- de Vaucouleurs, G., de Vaucouleurs, A., Corwin, Jr., H. G., et al. 1991, Third Reference Catalogue of Bright Galaxies. Volume I: Explanations and references. Volume II: Data for galaxies between 0^h and 12^h. Volume III: Data for galaxies between 12^h and 24^h.
- Elmegreen, B. G. & Elmegreen, D. M. 2006, *ApJ*, 650, 644
- Freudling, W., Romaniello, M., Bramich, D. M., et al. 2013, *A&A*, 559, A96
- Gamow, G. 1946, *Physical Review*, 70, 572
- Gilmore, G. & Reid, N. 1983, *MNRAS*, 202, 1025
- Holwerda, B. W., Keel, W. C., Williams, B., Dalcanton, J. J., & de Jong, R. S. 2009, *AJ*, 137, 3000
- Hubble, E. P. 1925, *ApJ*, 62, 409
- Johnston, K. V., Bullock, J. S., Sharma, S., et al. 2008, *ApJ*, 689, 936
- Kormendy, J. & Kennicutt, Jr., R. C. 2004, *ARA&A*, 42, 603
- Kuijken, K. & Dubinski, J. 1995, *MNRAS*, 277, 1341
- Langer, W. D., Pineda, J. L., & Velusamy, T. 2014, *A&A*, 564, A101
- Le Fèvre, O., Saisse, M., Mancini, D., et al. 2003, in *Society of Photo-Optical Instrumentation Engineers (SPIE) Conference Series*, Vol. 4841, Instrument Design and Performance for Optical/Infrared Ground-based Telescopes, ed. M. Iye & A. F. M. Moorwood, 1670–1681
- Lemaître, G. 1931, *Nature*, 127, 706
- Loebman, S. R., Roškar, R., Debattista, V. P., et al. 2011, *ApJ*, 737, 8
- Makarov, D., Prugniel, P., Terekhova, N., Courtois, H., & Vauglin, I. 2014, *A&A*, 570, A13
- Martinez-Valpuesta, I., Shlosman, I., & Heller, C. 2006, *ApJ*, 637, 214
- Mathewson, D. S., Ford, V. L., & Buchhorn, M. 1992, *ApJS*, 81, 413
- Minchev, I., Famaey, B., Quillen, A. C., et al. 2012, *A&A*, 548, A127
- Minchev, I., Martig, M., Streich, D., et al. 2015, *ApJ*, 804, L9
- Muñoz-Mateos, J. C., Sheth, K., Regan, M., et al. 2015, *ApJS*, 219, 3
- Narayan, C. A. & Jog, C. J. 2002, *A&A*, 394, 89
- Nyktyuk, T. V. & Mishenina, T. V. 2006, *A&A*, 456, 969
- Öpik, E. 1922, *ApJ*, 55, 406
- Peng, C. Y., Ho, L. C., Impey, C. D., & Rix, H.-W. 2010, *AJ*, 139, 2097
- Penzias, A. A. & Wilson, R. W. 1965, *ApJ*, 142, 419
- Qu, Y., Di Matteo, P., Lehnert, M. D., & van Driel, W. 2011, *A&A*, 530, A10
- Quinn, P. J., Hernquist, L., & Fullagar, D. P. 1993, *ApJ*, 403, 74
- Read, J. I., Lake, G., Agertz, O., & Debattista, V. P. 2008, *MNRAS*, 389, 1041
- Salo, H., Laurikainen, E., Laine, J., et al. 2015, *ApJS*, 219, 4
- Sandin, C. 2015, *A&A*, 577, A106
- Schönrich, R. & Binney, J. 2009, *MNRAS*, 396, 203
- Sheth, K., Regan, M., Hinz, J. L., et al. 2010, *PASP*, 122, 1397
- Skrutskie, M. F., Cutri, R. M., Stiening, R., et al. 2006, *AJ*, 131, 1163
- Springel, V. 2005, *MNRAS*, 364, 1105
- Toomre, A. 1977, in *Evolution of Galaxies and Stellar Populations*, ed. B. M. Tinsley & R. B. G. Larson, D. Campbell, 401
- Tsikoudi, V. 1979, *ApJ*, 234, 842
- Vazdekis, A., Sánchez-Blázquez, P., Falcón-Barroso, J., et al. 2010, *MNRAS*, 404, 1639
- Vera-Ciro, C., D’Onghia, E., Navarro, J., & Abadi, M. 2014, *ApJ*, 794, 173
- Villumsen, J. V. 1985, *ApJ*, 290, 75
- Yoachim, P. & Dalcanton, J. J. 2006, *AJ*, 131, 226
- Yoachim, P. & Dalcanton, J. J. 2008a, *ApJ*, 683, 707
- Yoachim, P. & Dalcanton, J. J. 2008b, *ApJ*, 682, 1004
- Zaritsky, D., Courtois, H., Muñoz-Mateos, J.-C., et al. 2014, *AJ*, 147, 134